Ann. Rev. Phys. Chem. 1982. 33:63–87

DYNAMICS OF MOLECULES IN CONDENSED PHASES: PICOSECOND HOLOGRAPHIC GRATING EXPERIMENTS

M. D. Fayer

Department of Chemistry, Stanford University,
Stanford, California 94305

INTRODUCTION

The development of laser equipment that can operate routinely in the subnanosecond (and more recently in the subpicosecond) time regimes has made possible the investigation of a wide variety of fast chemical, physical, and biophysical processes. Most of the successful picosecond time scale experiments, although very sophisticated in technique, have utilized the basic approaches that have been applied on slower time scales. One method involves monitoring time-resolved fluorescence following picosecond excitation (1–3). Since the time scale of interest is very short, techniques such as single photon counting, streak cameras, and fluorescence mixing have been employed to provide the necessary time resolution of the fluorescence. In many other experiments, the picosecond probe pulse technique has been used to examine changes in a systems absorption following picosecond optical excitation (4, 5).

In this article I discuss a different approach to the application of subnanosecond laser pulses to the investigation of molecular and excited state dynamics. This involves the optical generation of a transient holographic diffraction grating in a sample, and the observation of various time and frequency dependent phenomena via subsequent Bragg diffraction from the induced grating. The basic experiment works in the manner illustrated in Figure 1. Two time coincident picosecond laser pulses of the same wavelength are crossed inside of the sample to set up an optical

0066-426X/82/1101-0063$02.00

interference pattern. The fringe spacing, d, of the interference pattern is determined by the angle between the beams, θ, and the wavelength, λ, of the excitation pulses, i.e.

$$d = \lambda / 2\sin(\theta/2). \quad 1.$$

The interaction of the radiation field with the sample can produce a number of different changes in the sample, depending on the nature of the sample and the wavelength, λ. As discussed in the examples below, in which the samples are solids or liquids, electronic excited states can be produced (6), internal molecular vibrations can be excited (7), or acoustic waves, i.e. phonons, the collective vibrations of the medium, can be generated (7–11). In some experimental situations, more than one of the above types of excitations are simultaneously produced (11).

In all cases, the excitations generated in the sample have a spatial periodicity that mimics the periodicity of the optical interference pattern used to excite the sample. Excitation results in a spatially periodic change in the physical properties of the system. This in turn produces a periodic variation in the sample's complex index of refraction, **n** (11),

$$\mathbf{n} = n + iK. \quad 2.$$

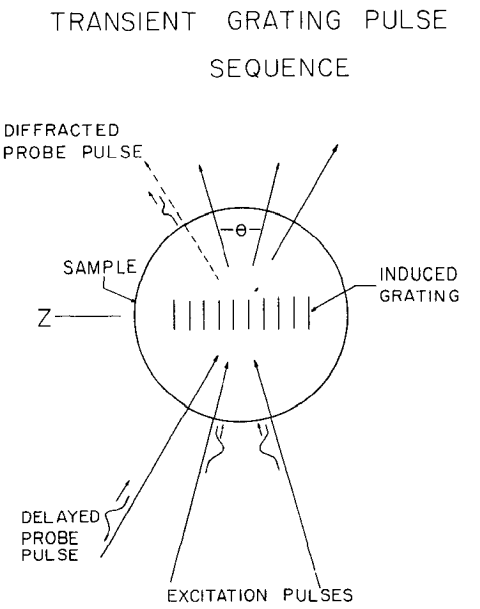

Figure 1 Schematic illustration of the transient grating experiment. Interference between the incoming excitation pulses results in an oscillatory density of excited states, which Bragg-diffracts the subsequent probe pulse. The diffracted probe is the signal, which reflects the time evolution of the excited state population.

The periodic variation in **n** acts as a Bragg diffraction grating for a picosecond probe pulse (11) (see Figure 1). The probe pulse is brought into the sample to meet the Bragg diffraction condition for the holographic transient grating produced by the excitation beams. A part of the probe pulse is diffracted and leaves the sample in a unique direction as a collimated beam. The intensity of the diffracted beam is the observable in the transient grating experiment. The probe pulse can be delayed various amounts in time, and the intensity of the diffracted beam as a function of probe pulse delay can be related to the system's dynamics (6). In addition, the probe pulse can be brought in at a fixed delay time, and the wavelength of either the probe (11) or excitation beams (7) can be varied. In this manner various types of spectroscopic measurements can be made.

Examples of the various types of experiments are presented below. These experiments include measurements of excited state dispersion relations (11), electronic excited state energy transport and trapping (6), the optical generation and detection of ultrasonic waves (8–11), vibrational overtone spectra (7), crystalline elastic constants (8, 9), and photoelastic constants (7).

EXPERIMENTAL SETUP

All of the experiments discussed below were performed with some variation of the transient grating experimental setup illustrated in Figure 2. The laser is a continuously pumped Nd:YAG system that is acousto-optically mode-locked and Q-switched to produce high repetition rate (400 Hz), high power infrared (1.06 μm) picosecond pulses. The laser output is a train of about 40 mode-locked pulses, 5.7 nsec apart, with $\sim$1.4 mJ total energy. A large pulse from the train is selected by a Pockels cell with avalanche transistor driver. The single pulse is frequency doubled using CD*A to give a 20 μJ, 80 psec, transform-limited, TEM_{00} pulse at 532 nm. This passes through a 50% beam-splitter to create the two excitation pulses, which travel equal distances and are focused into the sample.

The unused IR pulse train comes off a reflecting polarizer into another CD*A doubler crystal, and the 532 nm light is used to synchronously pump a dye laser that is spectrally narrowed and tuned by two intracavity etalons. The dye laser is cavity dumped using another Pockels cell with avalanche transistor driver to give a 10 μJ, 30 psec pulse with a spectral width of $\sim$1 cm^{-1}. Synchronization of the two Pockels cells is obtained by a single avalanche transistor, which itself is triggered by the IR pulse train. The dye laser output travels a variable distance controlled

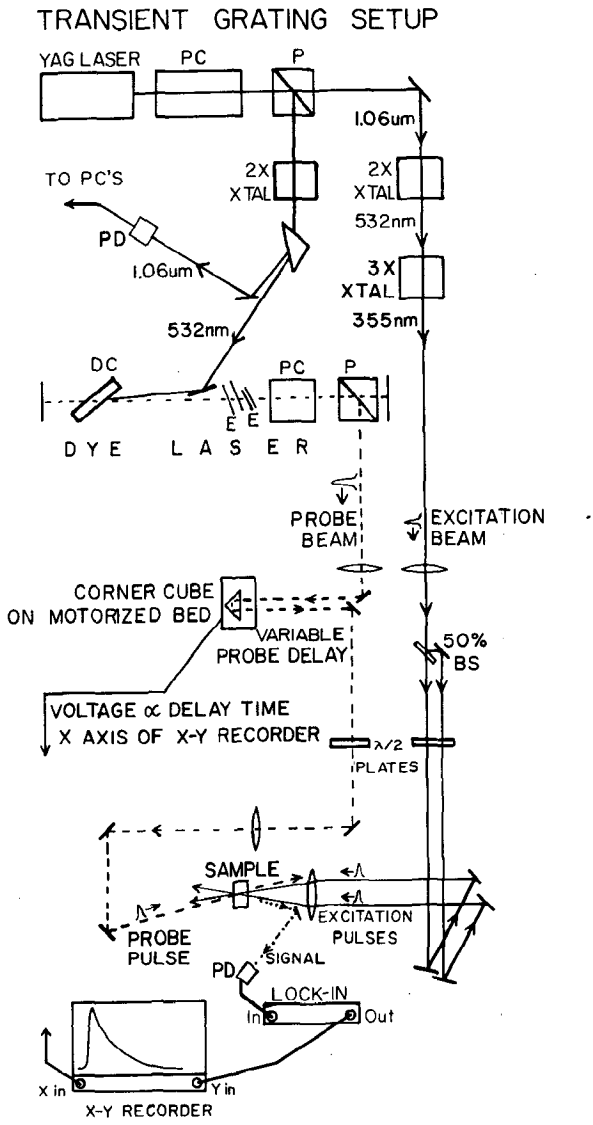

Figure 2 Transient grating experimental setup. A single 1.06 μm pulse is selected from the YAG mode-locked pulse train. Generally, one of its harmonics is employed (shown here with 3×), although in some experiments the fundamental or a tunable mode-locked dye laser pulse may be used. The single pulse is then split into two excitation pulses. These excitation pulses are recombined at the sample, creating the transient grating. The remainder of the pulse train is frequency doubled to synchronously pump a tunable dye laser whose output probes the grating after a variable delay. In some experiments a YAG harmonic is used as a probe. The Bragg-diffracted part of the probe pulse is the transient grating signal. PC ≡ Pockels cell; P ≡ polarizer; PD ≡ photodiode; DC ≡ dye cell; E ≡ etalon; BS ≡ beamsplitter.

by a motorized delay line consisting of a corner cube drawn along a precision optical rail. It probes the grating at an angle satisfying the Bragg diffraction condition. In some of the experiments described below, the dye laser was used for tunable excitation and the probe wavelength was 532 nm. In other experiments, a single color, either dye laser or YAG laser (or a harmonic), was used for both excitation and probing.

A large area photodiode and a lock-in amplifier are used to detect the diffracted signal beam. For time independent experiments, the probe pulse is delayed an appropriate fixed amount and either the probe or excitation wavelength is tuned. The diffracted intensity is recorded as a function of wavelength. For time dependent measurements the lock-in amplifier output drives the y-axis of an x-y recorder. The x-axis is driven by a variable voltage derived from a ten-turn potentiometer connected to the delay line motor, providing the time scale. When the delay line is run, the time dependent diffracted signal is recorded directly on the x-y recorder. If significant data manipulation is required, a minicomputer using analog to digital converters is used to record the time dependent signal for subsequent data analysis.

ELECTRONIC EXCITED STATE PHASE AND AMPLITUDE GRATINGS: PROBE WAVELENGTH DEPENDENCE NEAR A STRONG TRANSITION

As discussed above, the diffraction of the probe pulse from the optically induced grating is due to a spatially periodic variation in the complex index of refraction, $\mathbf{n}$ (Eq. 2). The diffraction efficiency is proportional to the difference in $\mathbf{n}$ at the grating peaks and nulls (11). In this section I consider the diffraction efficiency from a grating that arises from the production of electronic excited states by the excitation pulses (11). Generation of electronic excited states causes changes in both the real and the imaginary parts of the index of refraction and, in general, both the spatial variation in n and K give rise to diffraction efficiency (12).

The change, $\Delta K_{ex}(\omega)$, in the imaginary part of $\mathbf{n}$ due to the excited states is related to the peak-null difference in absorption at the probe wave length, ω. $\Delta K_{ex}(\omega)$ gives rise to an amplitude grating. For ω on or near an absorption peak, $\Delta K_{ex}(\omega)$ can be substantial. Thus the probe pulse experiences alternating regions of high and low optical transmission. This periodic variation in absorption produces, in effect, a multislit diffraction, i.e. an amplitude grating.

The change, $\Delta n_{ex}(\omega)$, in the real part of $\mathbf{n}$ due to excited states is related to the peak-null difference in optical dispersion at the probe

wavelength, ω. $\Delta n_{ex}(\omega)$ gives rise to a phase grating. In the vicinity of an absorption peak, the probe pulse experiences a periodic variation in the velocity of light-producing alterations in the probe wavefront's phase. This phase variation gives rise to diffraction.

For a sinusoidal volume grating, the diffraction efficiency, $\eta(\omega)$, is (11)

$$\eta(\omega) = e^{-\frac{2.3 D_{av}(\omega)}{\cos\theta}} \left[\sinh^2 \frac{\Pi T \Delta K(\omega)}{\lambda \cos\theta} + \sin^2 \frac{\Pi T \Delta n(\omega)}{\lambda \cos\theta} \right]. \quad 3.$$

The first term in brackets determines the amplitude grating diffraction, $\eta_a(\omega)$, and the second determines the phase grating diffraction, $\eta_p(\omega)$. T is the sample thickness. $D_{av}(\omega)$ is an average optical density adjusted such that the exponential term describes the absorptive loss. In most experimental situations, the total diffraction efficiency is not large, ($\eta < 0.01$) and Eq. 3 can be approximated by (11)

$$\eta(\omega) = e^{-\frac{2.3 D_{av}(\omega)}{\cos\theta}} \left(\frac{\Pi T}{\lambda \cos\theta} \right)^2 \left\{ [\Delta K(\omega)]^2 + [\Delta n(\omega)]^2 \right\}. \quad 4.$$

The grating diffraction efficiency given by Eq. 4, which depends on $\Delta K(\omega)$ and $\Delta n(\omega)$, must now be related to the excited state concentrations produced by transient grating excitation. This is accomplished by describing the system with a damped harmonic oscillator model for the Kramers-Kronig relations (13). For the probe wavelength, ω, near a single strong optical transition (11), e.g. the probe is tuned near the S_0 to S_1 absorption of a solute molecule in a transparent solvent (as discussed below),

$$\Delta n_{ex}(\omega) = -\frac{N_1}{N_0} \frac{2(\omega_0 - \omega)}{\gamma_0} K_0(\omega) \quad 5a.$$

$$\Delta K_{ex}(\omega) = -\frac{N_1}{N_0} K_0(\omega) \quad 5b.$$

with

$$K_0(\omega) = K_0(\omega_0) \frac{\gamma_0^2}{4(\omega_0 - \omega)^2 + \gamma_0^2} \quad 6a.$$

and

$$K_0(\omega_0) = \frac{1}{2n_0} N_0 \frac{e^2}{3\varepsilon_0 m} \frac{f_0}{\gamma_0 \omega_0}. \quad 6b.$$

N_0 is the number density of absorbing molecules and N_1 is the number density of excited states at the grating peaks. ω_0 is the frequency of the absorption maximum of the transition being probed and γ_0 is its line

width (FWHH). n_0 is the bulk index of refraction (excluding the contribution from the transition being probed), and f_0 is the oscillator strength of the transition being probed. e, m, and ε_0 are the electron charge, electron mass, and the permitivity of free space, respectively.

From Eq. 4 with Eqs. 5 and 6 it can be seen that the signal in a transient grating experiment depends on changes in both the optical density of the sample ($\Delta K_{ex}(\omega)$) and the dispersion of the sample ($\Delta n_{ex}(\omega)$) due to the production of excited states. A conventional picosecond probe pulse experiment only depends on the changes in the optical density upon excitation. If this were the case for a transient grating experiment, the diffraction efficiency (amplitude grating only) would have a probe wavelength dependence proportional to the absorption spectrum squared, i.e. $[\Delta K_{ex}(\omega)]^2$. The amplitude-grating contribution is peaked at the absorption maximum and falls off rapidly at longer and shorter wavelengths. The phase grating contribution, $[\Delta n_{ex}(\omega)]^2$, is zero at the absorption maximum and is peaked at the half heights of the absorption line on both sides of the absorption maximum.

The above considerations are demonstrated experimentally in Figure 3 (11). The sample is a mixed molecular crystal (solid solution) of pentacene in the host *p*-terphenyl. The *inset* in the figure shows the absorption spectrum. The transient grating excitation employed doubled Nd:YAG pulses at 532 nm. The diffraction efficiency $\eta_{ex}(\omega)$ due to the resulting excited state grating was measured at fixed time delay (500 psec) as a function of probe wavelength using tunable dye laser pulses as the probe. The *solid line* through the experimental points (Figure 3a) represents the experimentally measured diffraction efficiency in the vicinity of the pentacene S_0 to S_1 absorption. The *dashed line* shows the theoretically predicted diffraction efficiency from Eq. 4 with Eqs. 5 and 6. The agreement between the two curves is excellent, especially on the red side of the origin, which is spectrally isolated. The blue side of the origin is influenced by the next absorption band (see inset spectrum), which was not included in the calculation.

The diffraction efficiency is not adequately described by amplitude grating effects alone (the *dash-dot curve* in Figure 3a). At the absorption peak, the phase-grating contribution vanishes and thus the amplitude grating, η_a, accounts for all of the observed signal. η_a scales as the square of the absorption strength, and the *dash-dot curve* in Figure 3a was plotted from the inset absorption spectrum. The difference between this curve and the observed signal gives the diffraction resulting from phase-grating effects. This is plotted in Figure 3b (the *solid curve* through the experimental points). The phase-grating contribution rises from zero at the absorption peak to maxima at the halfwidths, then gradually decreases, as theoretically predicted (the *dashed curve*). The asymmetry in

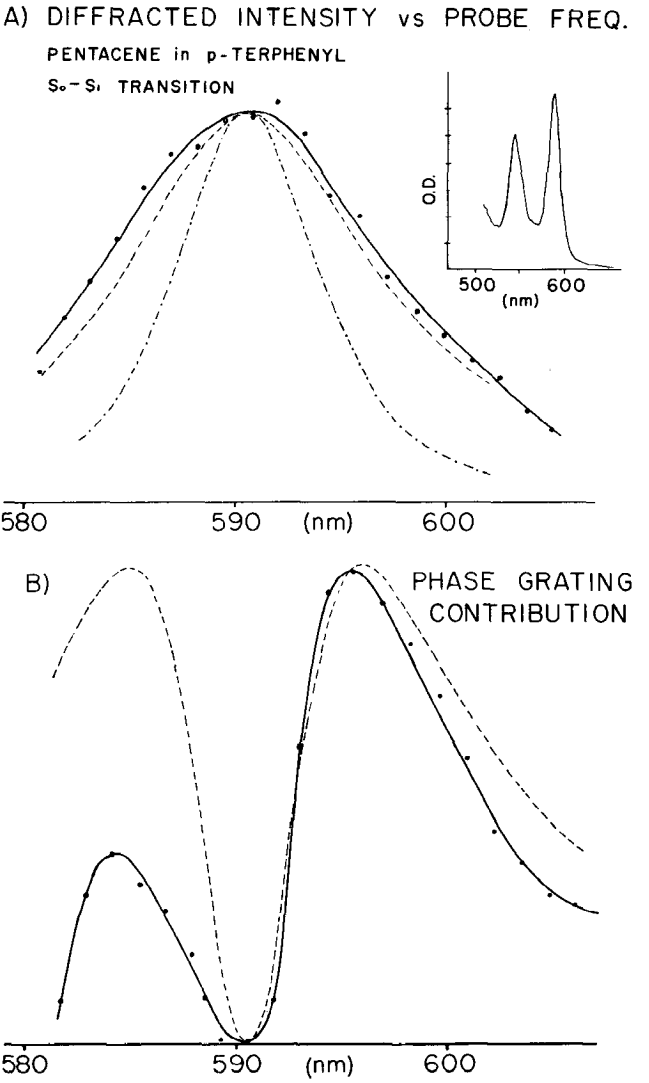

Figure 3 (*a*) The circles with the solid line are the experimentally measured excited state grating diffraction intensity as a function of probe wavelength near the S_0 to S_1 transition of pentacene in a crystal of *p*-terphenyl. The *dashed curve* is theoretically calculated from the absorption spectrum (*inset*). The *dash-dot curve* is the calculated amplitude grating contribution to the diffraction efficiency. This demonstrates the significant contribution of phase grating effects. (*b*) The points with the *solid line* are the phase-grating contribution to the diffraction intensity obtained by subtracting the curves in (*a*). The predicted *m* shape curve associated with excited state phase grating diffraction is clearly observed. The *dashed curve* is theoretically calculated from the absorption spectrum. On the red side, where the transition is isolated, the agreement is good. On the blue side, interference from the next spectral peak (see inset), which was not included in the calculation, influences the dispersion effect.

$\eta_p(\omega)$ results from the influence of the absorption band (see inset spectrum) on the blue side of the origin. This band was not included in the theoretically calculated curve.

These results confirm the theoretical predictions of the contributions of excited state amplitude and phase gratings to the transient grating diffraction efficiency. Although excited state phase gratings have been discussed by a number of authors (14), experimental observations have been sketchy. The results presented here provide the clearest characterization of the wavelength dependence of excited state phase-grating diffraction. In many experimental situations, failure to account properly for both phase- and amplitude-grating effects can lead to erroneous interpretations of data. This can be true in more general four-wave mixing experiments as well as in transient grating experiments.

TIME DEPENDENT EXCITED STATE GRATING EXPERIMENTS: EXCITED STATE TRANSPORT AND TRAPPING IN CONCENTRATED DYE SOLUTIONS

As with picosecond probe pulse experiments, picosecond transient grating experiments can be used to examine time dependent dynamics of excited state systems. As can be seen from Eqs. 4, 5, and 6, the signal, i.e. the diffraction efficiency, depends on $(N_1)^2$, the square of the number of excited states at the grating peaks. In the absence of any other process, the time dependent signal, $S(t)$, at a fixed probe wavelength will be determined by the excited state lifetime,

$$S(t) = S(0)e^{-2Kt}. \qquad 7.$$

K is the rate constant for the decay of the excited states. The factor of two in the exponential arises because the signal depends on $[N_1(t)]^2$. Thus for an exponential decay of the excited state population, the transient grating signal will decay exponentially with twice the rate constant.

Virtually any experiment that can be performed with a picosecond probe pulse approach can also be performed with a picosecond transient-grating experiment. In many instances there are significant advantages to using the transient-grating approach. For some types of experiments, e.g. measurement of long-range transport of electronic excitations, the transient-grating method can be applied where probe pulse or fluorescence experiments are not applicable. My research group is currently employing transient-grating experiments involving excited

states to examine rotational reorientation of molecules in solution, electronic excited state energy transport in dilute solutions, excited state transport in biological systems related to photosynthesis, excited state transport in polymer systems, excited state transport in mixed and pure molecular crystals, and transport and trapping of excited states in polymer systems and concentrated dye solutions. To illustrate the basic ideas, excited transport and trapping in concentrated dye solutions, which are responsible for fluorescence quenching, are discussed here (6).

The experimental evidence suggests that three radiationless processes govern the disposition of electronic excited state energy in concentrated dye solutions. These three processes are energy transfer between dye molecules (1, 15), trapping by dimers (16, 17), which have states of lower energy, and radiationless relaxation (18) of the dimer excited state. A simple model provides a microscopic dynamical picture of fluorescence quenching (19) in concentrated dye solutions. The results given here directly relate to concentration quenching in dye lasers, an important limiting effect (19). In addition, the phenomena under consideration are the important initial steps in photosynthesis, i.e. electronic excitation transfer between chlorophyll chromophores and trapping on reaction centers (dimers) (20–22). Qualitatively, the concentration dependent processes that combine and result in fluorescence quenching work in the following manner. At very low concentration, a dye solution absorbs light and fluoresces. At moderate concentrations, electronic excited state energy transport occurs due to dipole-dipole interactions between the dye molecules (23). The energy transport causes fluorescence depolarization effects (3) but does not affect the fluorescence quantum yield. As the concentration is increased further, ground state dimer formation begins (24, 25) and the rate of energy transport continues to increase. By dimers we mean aggregates of two dye molecules that have distinct spectral and other characteristics. Rapid transport among the monomers allows an excitation to find a dimer and become trapped on it. The experiments indicate that back transfer from the excited dimer to monomers is negligible. Once the excitation is trapped on a dimer, rapid radiationless relaxation to the ground state occurs, and the fluorescence is quenched.

The concentration dependence of the fluorescence quenching is determined by the concentration dependence of the trapping. The trapping rate depends on both the dimer concentration and the concentration dependent rate of energy transport. The model predicts that the trapping rate varies approximately as the cube of the dye concentration. Therefore the onset of fluorescence quenching with increasing concentration is very rapid.

Experimentally, the onset of trapping by dimers manifests itself as an apparent reduction in the excited state lifetime. In the limit that energy transport becomes extremely rapid, the trapping occurs on a time scale that is short relative to the dimer lifetime, and the excited state population decays with the dimer lifetime. In the two systems studied, Rhodamine 6G (R6G) in glycerol and R6G in ethanol, the dimer lifetimes are 830 psec and <50 psec, respectively. Presumably, the dimers have faster radiationless relaxation rates than the monomers because of the loose nature of the dimer complexes. The dimers undergo rapid configurational changes that enhance the radiationless relaxation rates. This is consistent with the longer dimer lifetime in the glycerol solvent. Since glycerol is much more viscous than ethanol, it will "hold" the dimer complex more rigidly and therefore slow radiationless relaxation.

A formally correct, accurate treatment of this problem involves the solution of the Master Equation for excited state transport and trapping in an ensemble of randomly distributed dye molecules and dimer traps in solution. A solution to the Master Equation has recently been obtained using a diagrammatic self-consistent approach to obtain the Green function describing the transport and trapping problem (16). Description of this formalism is beyond the scope of this discussion; rather a heuristic, qualitatively correct, analysis (6) in terms of a simple set of rate equations is presented. These rate equations employ a trapping rate constant. The full diagrammatic Green function treatment confirms the results presented here; however, trapping is not governed by a rate constant, but involves a time dependent trapping rate function.

In the simple model the rate equations governing the excited state populations are:

$$dM^*/dt = -K_M M^* - K_T M^* \qquad 8a.$$

$$dD^*/dt = -K_D D^* - K_T M^*. \qquad 8b.$$

M^* is the concentration of excited monomers, and D^* is the concentration of excited dimers. K_M is the rate constant for decay of excited monomers to the ground state by radiative and nonradiative processes, and K_D is the analogous rate constant for decay of dimers to the dimer ground state. K_T is the trapping rate constant.

As discussed above, the transient grating signal depends on the square of the excited state concentrations, $[N_i(t)]^2$, i.e.

$$S(t) = A[N_i(t)]^2 \qquad 9.$$

where A contains all of the time independent parameters such as beam

geometries and $N_1(t) = M^* + D^*$, the sum of the excited monomer and dimer concentrations. Solution of the rate equations yields

$$N_1(t) = M_0^*\left[\exp\left[-(K_M + K_T)t\right] + \left[K_T/(K_M + K_T - K_D)\right] \times \left\{\exp(-K_D t) - \exp\left[-(K_M + K_T)t\right]\right\}\right]. \quad 10.$$

$N_1(t)$ is the time-dependent function determined experimentally from $S(t)$. It is informative to note some special cases of Eq. 10. If K_T is very small, trapping is negligible and $N_1(t)$ decays exponentially with the monomer rate constant, K_M. If $K_D \gg K_M, K_T$, then $N_1(t)$ decays exponentially with a rate constant $(K_M + K_T)$. And if $K_T \gg K_M, K_D$, excitations are immediately trapped by dimers and $N_1(t)$ decays exponentially with the dimer rate constant, K_D.

In general, trapping is characterized by a time-dependent trapping rate function (16, 26). Trapping occurs when an excitation has visited enough distinct sites so that on the average it has sampled one trap species. For a random walk on an isotropic three dimensional lattice, the number of distinct sites visited increases linearly with time (27). Therefore, trapping can be characterized by a trapping rate constant which depends on the site-to-site hopping time. I assume that trapping can also be characterized by a trapping rate constant in the solution systems discussed here. At high concentration, this is reasonable since transport is basically diffusive and isotropic in three dimensions. Although we do not have a periodic lattice, the randomness in spatial distribution of the sites (dye molecules) associated with a solution is taken into consideration in the calculation of the hopping time.

The above considerations lead to the following expression for the trapping rate constant (6), K_T:

$$K_T = \left(\frac{Pq}{h_1 M_1^2}\right) M^3. \quad 11.$$

K_T depends on the cube of the dye concentration, M. The other parameters are constants. q is the monomer-dimer equilibrium constant. h_1 is the site-to-site hopping time and M_1 is the dye concentration, both for a solution with the Forster unitless concentration, $C = 1$ (6). P is the probability that on any step a distinct site is visited. It corrects for the return to previously visited sites. For an isotropic three dimensional random walk on a lattice, $P \approx 0.7$, and I use this value here.[1] Equation 11

[1]Our P corresponds to Montroll's $1/u_0$, which is 0.65946 for a simple cubic lattice. This value was misprinted originally, but the correct value $u_0 = 1.5164$ was used in later works. See, for example, Ref. (28).

shows that this model predicts that the trapping rate constant depends on the concentration cubed. Thus, trapping increases very rapidly with concentration.

Examination of $N_1(t)$, Eq. 10, which gives the time-dependent signal, shows that in general the decays are nonexponential. In the data analysis the following procedure is employed. The experimental decays are plotted on log paper and a decay constant is determined for each concentration. These are then compared to a theoretical effective decay constant, K_{eff}, obtained from Eq. 10 by finding the time required for $N_1(t)$ to fall to $1/e$. Thus

$$K_{\text{eff}} = 1/t^{\dagger} \tag{12.}$$

with $t^{\dagger}$ obtained from Eq. 10 by

$$N_1(t^{\dagger}) = 1/e\left[N_1(0)\right]. \tag{13.}$$

Transient grating experiments were performed on a series of solutions of Rhodamine 6G in glycerol ranging in concentration from 8.7×10^{-4} m/l to 0.05 m/l. A typical result and log plot are shown in Figure 4. In all cases the data appeared to decay exponentially for several lifetimes. Thus, the decay could be characterized by an effective rate constant, K_{eff}, as discussed above. A plot of K_{eff} vs R6G concentration is shown in Figure 5. First consider the qualitative features of the concentration dependence. At low concentration, K_{eff} is concentration independent and

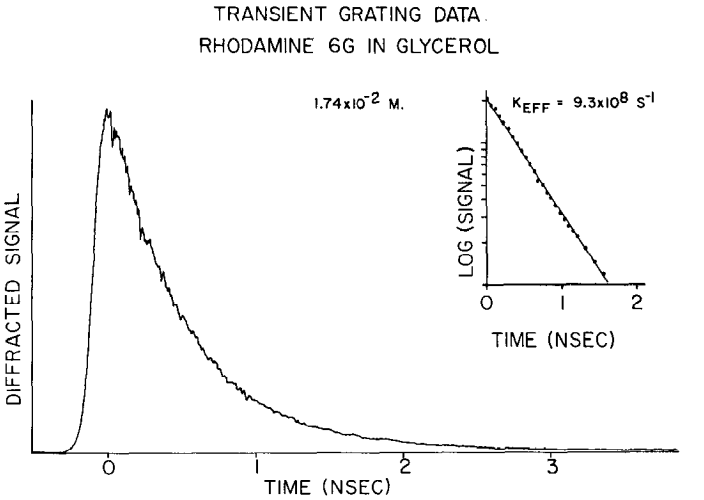

Figure 4 Transient grating results for Rhodamine 6G in glycerol. Probe wavelength = 560 nm. Inset shows the log of the data vs time. The effective decay constant for this data set is $K_{\text{eff}} = 9.3\times10^{8}\ \text{s}^{-1}$.

given by the monomer decay rate: $K_{eff} = K_M = 3.3 \times 10^8 s^{-1}$. This represents the limit $K_T = 0$, i.e. no trapping, since there are few dimers and transport is relatively slow. At high concentration, K_{eff} is essentially concentration independent and given by the dimer decay rate: $K_{eff} \approx K_D = 1.2 \times 10^9\ s^{-1}$ and the dimer lifetime is 830 psec. This corresponds to the limiting case $K_T \gg K_D, K_M$ (instantaneous trapping), which occurs at high concentration since the dimer population is substantial and energy transfer is fast.

In addition to affecting excited state dynamical processes, dimer formation should give rise to changes in the ground state absorption spectra of the solutions (24, 25). Spectra of solutions of many concentrations were examined, and it was found that the onset of spectral changes coincides with the onset of changes in the excited state decay rate. This clearly demonstrates that the concentration dependence of the decay rate is due to changes in the ground state molecules and not to processes such as excimer formation that only affect the excited states.

Detailed comparison of the model and the experimental data is given in Figure 5. The monomer and dimer decay rates were determined from the transient grating (TG) data at low and high concentration, respec-

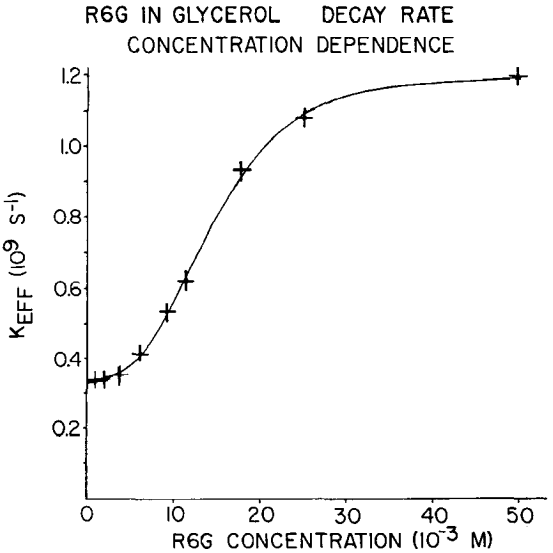

Figure 5 Effective decay constant, K_{eff} vs concentration of Rhodamine 6G in glycerol. + indicates experimental data. As the R6G concentration increases, excited state transport and trapping by R6G dimers becomes increasingly rapid. Fast radiationless relaxation by the dimers decreases the excited state lifetime and quenches fluorescence. The *solid curve* is calculated.

tively. Since the equilibrium constant, q, is not known, TG data at a single intermediate concentration was used to determine K_T. Decay constants K_{eff} were then calculated at other concentrations by scaling K_T as the concentration cubed and using Eq. 10. The calculated values of K_{eff} as a function of concentration yielded the curve (*solid line*) shown in Figure 5. The curve fits the experimentally measured decay constants over the range of concentrations, indicating that the microscopic model is basically correct.

Knowing K_T allows calculation of the equilibrium constant for dimer formation from Eq. 10 since the other parameters are known. An equilibrium constant $q = 9.7$ 1/m was obtained. Equilibrium constants for various solutions of R6G in glycerol-water mixtures have been determined from concentration dependent absorption spectra to range from 28 1/m in the solution with the most water to 11 1/m in the solution with the least water (25). The equilibrium constant that resulted from the time-dependent measurements is consistent with these values. This provides additional support for the basic model.

Similar experiments were performed for the system R6G in ethanol (6). At low concentration the rate constant is determined by the monomer decay rate: $K_{eff} = K_M = 2.7 \times 10^8$ s^{-1}. As the concentration rises, the decay rate rapidly increases. The measurement at the highest concentration is instrumentally limited by the laser pulse duration. The excited state decay constant at high concentration is at least 2×10^{10} s^{-1}, i.e. the lifetime is less than 50 psec. This is in marked contrast to the glycerol solutions, in which the dimer lifetime is 830 psec.

Clearly the radiationless relaxation rates of the loosely bound dimer are influenced by the solvent viscosity. The low viscosity of ethanol permits rapid configurational fluctuations that lead to very fast radiationless relaxation. The fluctuations occur more slowly in glycerol, and thus the dimer lifetime is longer.

These results directly apply to concentration-dependent fluorescence quenching in dye solutions. Trapping on dimers, which increases as the cube of the dye concentration, leads to fast radiationless relaxation and thus quenches fluorescence. The solvent-dependent dimer lifetime alsc influences fluorescence quenching. In high concentration R6G in ethanol solutions, fluorescence is completely quenched since the dimer radiationless relaxation rate is extremely fast. In high concentration glycerol solutions, fluorescence is only partially quenched since the dimer decay rate is only four times faster than the monomer decay rate. This allows some radiative relaxation to occur.

Transient grating experiments were used in these measurements for two reasons. First, a TG experiment is inherently more sensitive than a

probe pulse experiment, although in principle both could provide the same information about the processes under consideration here. In a probe pulse experiment, small changes in an intense beam provide the information. In a grating experiment there is a dark background. The entire diffracted beam is the signal. In a probe pulse experiment in which F is the fraction change in the probe, roughly F^2 of the probe would be diffracted in a grating experiment. In a probe pulse experiment it is extremely difficult to see a change of $F = 0.001$. However, in a grating experiment it is straightforward to detect 10^{-6} diffraction of the probe since it is against a dark background. We found in probe pulse experiments that the highly concentrated samples required very large excitation power densities to achieve sufficient bleaching of the ground state population to give reasonable signal. These very high power densities resulted in anomalous power-dependent decays. In the grating experiments it was possible to use low power densities and still retain good signal-to-noise ratios, making the experiments possible. The second advantage of the grating method is a reduction in the problem of reabsorption of fluorescence in concentrated samples. In a grating experiment, the relevant reabsorption path length is a few fringe spacings, i.e. a few microns. In a probe pulse experiment, reabsorption must not occur in a length corresponding to the probe spot size, $\sim 100\ \mu$m. In addition, there are a number of types of experiments, such as the measurement of long-range transport processes (29) or the experiments described in the next section, which are only possible using the transient grating approach.

OPTICAL GENERATION AND DETECTION OF ULTRASONIC WAVES AND APPLICATIONS TO PHYSICAL MEASUREMENTS

Optical generation of ultrasonic waves has been of interest to workers in nonlinear optics, acoustics, and condensed matter spectroscopy for some time (30–36). The interaction between light and material acoustic fields is of interest in its own right; furthermore, efficient light to ultrasound conversion holds promise for a variety of scientific and practical applications. Here, a convenient method for optical excitation of coherent acoustic waves in transparent or light-absorbing liquids and solids is described. The acoustic frequency can be continuously and easily varied from about 3 MHz to 30 GHz with our experimental apparatus, and a considerably wider range should be possible. In anisotropic media (crystals, liquid crystals, stretched films, etc) any propagation direction can be selected.

The technique, called Laser Induced Phonons (LIPS), is based on the transient grating experiment (Figure 1) and works as follows. Two time-coincident laser pulses of approximately 100 psec duration intersect inside the sample, setting up an optical interference pattern, i.e. alternating intensity peaks and nulls. Energy deposited into the system via optical absorption or stimulated Brillouin scattering results in the launching of counterpropagating ultrasonic waves (phonons) whose wavelength and orientation match the interference pattern geometry. The acoustic wavelength is given by Eq. 1. With the Nd:YAG laser system in our laboratory we can vary d between 1 mm and 0.1 μm, i.e. over a range of four orders of magnitude. In most materials this corresponds to tunable acoustic frequencies from about 3 MHz to 30 GHz.

The acoustic wave propagation, which continues long after the excitation pulses leave the sample, causes time-dependent, spatially periodic variations in the material density, and since the sample's optical properties (real and imaginary parts of the index of refraction) are density-dependent, the irradiated region of the sample acts as a Bragg diffraction grating. This propagation of the optically excited ultrasonic waves can be optically monitored by time-dependent Bragg diffraction of a variably delayed probe laser pulse.

Diffraction from an ultrasonic wave grating can in principle arise from two distinct mechanisms: (a) changes in the number density of molecules, and (b) changes in the positions of resonances (density-dependent spectral shifts). Both of these could result in amplitude and phase grating diffraction. Under most conditions, phase grating diffraction due to changes in number density predominates (11), and in fact accounts for all acoustic diffraction devices and experiments realized to date. However, it appears that spectral shift effects could be observed in a LIPS experiment under the proper circumstances (11).

The effects of changes in number density are readily calculated. If the peak-null variation in strain is S, then the corresponding peak-null variation of the real and imaginary parts of $\mathbf{n}$ are, respectively (11),

$$\Delta n_d = -S\frac{(n_0^2-1)}{2n_0} \qquad 14a.$$

$$\Delta K_d = -SK_0(\omega). \qquad 14b.$$

These expressions are used with Eq. 4 to calculate the diffracted signal from an ultrasonic grating. It is clear that there will be a phase grating contribution due to density changes at any probe wavelength. However, there will only be amplitude grating diffraction when the probe frequency, ω, is on or near an absorption. Furthermore, it is found that the

amplitude contribution will always be small unless the transition is very strong. In the experiments discussed below, all of the ultrasonic gratings are phase gratings.

The mechanism by which LIPS ultrasonic waves are generated depends upon whether the sample is optically absorbing or transparent at the excitation wavelength. If the excitation pulses are absorbed into high-lying vibronic levels, rapid radiationless relaxation and local heating at the interference maxima (the transient grating peaks) occurs. Thermal expansion then drives material in phase away from the grating peaks and toward the grating nulls, setting up counterpropagating waves. The acoustic response to absorbed excitation pulses, in terms of relative material displacement (strain), has been shown to be (8–11)

$$S_{zz} = A\{\cos kz - \tfrac{1}{2}[\cos(\omega t + kz) + \cos(\omega t - kz)]\}$$
$$= A\cos kz(1 - \cos \omega t), \qquad 15.$$

where S_{zz} is the compressional strain along the z-direction, A is the amplitude of the acoustic disturbance, k is the grating (phonon) wave vector, and ω is the acoustic frequency. ($\omega/k = v_z$, the longitudinal speed of sound along the z-direction in the medium.) The excitation geometry is as shown in Figure 1. The acoustic disturbance in Eq. 15 can be viewed as a steady-state expansion (the *dc* term) plus a transient response (the counterpropagating waves). For simplicity we assume propagation of a single, longitudinal wave, although we (8–11) have demonstrated, and illustrate below, that in anisotropic media quasilongitudinal and quasitransverse waves can also be generated. Local changes in material density, ρ, are given by

$$\delta\rho = -\rho_0 S_{zz}, \qquad 16.$$

where ρ_0 is the normal density.

The excitation pulses are taken to be instantaneous and cross inside the sample at $t = 0$. At this time $\delta\rho = 0$ everywhere, i.e. the density is uniform. Material then moves away from the peaks and toward the nulls, causing the density at the peaks to decrease and the density at the nulls to increase. The density excursion is largest at $t = \pi/\omega$ (and $t = 3\pi/\omega$, $5\pi/\omega$, etc), and returns to normal at $t = 2\pi/\omega$, $4\pi/\omega$, etc (after each acoustic cycle). Thus the density at the grating peaks oscillates between normal and a reduced value, while the density at the grating nulls oscillates between normal and an increased value. The variably delayed probe pulse undergoes no diffraction at $t = 0$, $2\pi/\omega$, etc (uniform density), and is most strongly diffracted at $t = \pi/\omega$, $3\pi/\omega$, etc (maximum density excursion).

In samples that are transparent at the excitation wavelength, optical energy is coupled directly into the sample's acoustic field via stimulated Brillouin scattering (9, 10). This process takes advantage of the inherent spectral line width in the 100 psec excitation pulses. Higher frequency photons from each pulse are annihilated to create lower frequency photons in the opposite pulse and phonons of the difference frequency and wave vector in the medium. Counter-propagating waves (a standing wave) are thus produced. The acoustic response has been predicted earlier to be (9, 10)

$$S_{zz} = -\frac{B}{2}[\sin(\omega t + kz) + \sin(\omega t - kz)]$$
$$= -B\cos kz \sin \omega t, \qquad 17.$$

where B is the acoustic wave amplitude. Experimental observations of this acoustic response are presented below (7, 10). Notice that since there is no radiationless relaxation or heating, no static thermal expansion occurs. (Compare with Eq. 15.) The density at any point in the sample oscillates both above and below normal, and the density is normal everywhere ($\delta\rho \equiv 0$) at $t = 0, \pi/\omega, 2\pi/\omega$, etc (twice each acoustic cycle). Thus the variably delayed probe pulse undergoes no diffraction twice each acoustic cycle. The different time dependences of the diffracted signal arising from the two acoustic wave-generating mechanisms allow simple determination of the mechanism of phonon excitation in a LIPS experiment.

Figure 6 shows LIPS data from pure ethanol and from solutions of malachite green in ethanol. The 532 nm excitation light is absorbed by malachite green but not by ethanol. The grating fringe spacing is 2.47 μm and the speed of sound in ethanol is 1.16×10^5 cm/sec (37). The acoustic frequency is therefore $\omega = 2.95 \times 10^9$ s^{-1}, and the acoustic period $\tau_{ac} =$ 2.13 nsec. (The acoustic period is the time required for the ultrasonic waves to travel one fringe spacing.) Figure 6a shows LIPS data from pure ethanol. The important feature is the frequency of oscillations in the diffracted intensity. Signal vanishes every 1.07 nsec, or exactly twice each acoustic cycle. This indicates that the acoustic disturbance is as given in Eq. 17, and that simulated Brillouin scattering is responsible for acoustic wave production. This is to be expected since the green excitation light is not absorbed by pure ethanol.

Figure 6c shows data from a solution of 5×10^{-5} M malachite green in ethanol. This concentration is such that the acoustic disturbance due to optical absorption completely obscures that due to electrostriction. The diffracted intensity vanishes once each acoustic cycle, indicating that the

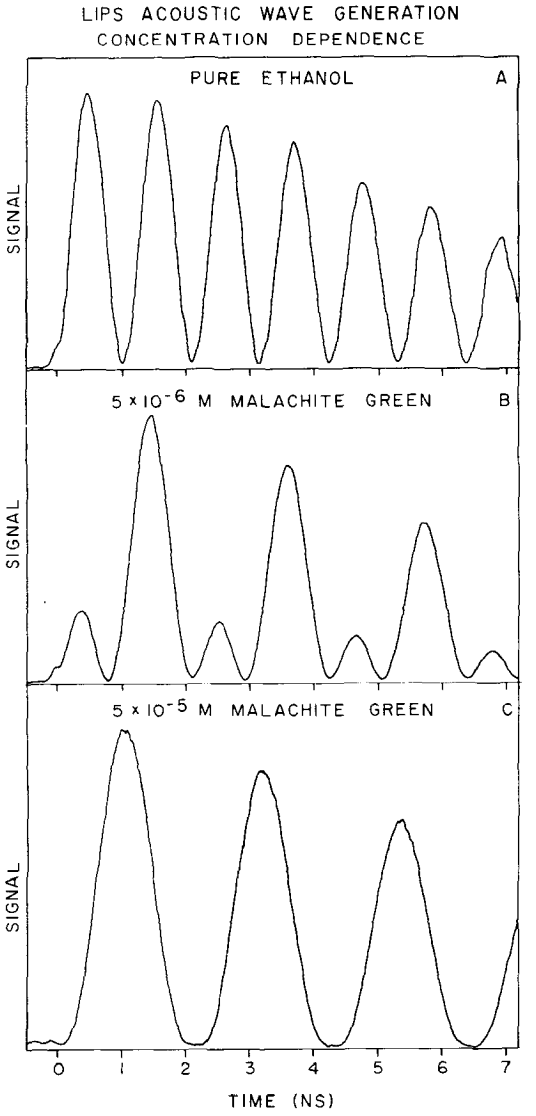

Figure 6 Laser Induced Phonons (LIPS) transient grating data from pure ethanol and solutions of malachite green in ethanol. Excitation $\lambda = 532$ nm; probe $\lambda = 566$ nm. Fringe spacing $d = 2.47$ μm; acoustic cycle $\tau_{ac} = 2.13$ nsec. Experimental conditions other than sample were identical throughout. (*a*) Pure ethanol. Electrostrictively generated standing wave causes diffraction intensity to oscillate twice each acoustic cycle. (*b*) 5×10^{-6} M malachite green in ethanol. Electrostriction and optical absorption produce comparable responses. (*c*) 5×10^{-5} M malachite green in ethanol. Optical absorption effects dominate. Diffracted signal oscillates once each acoustic cycle.

acoustic response is as given in Eq. 15. Figure 6b shows data from a solution of intermediate malachite green concentration. Optical absorption and electrostriction excite acoustic responses of comparable magnitudes, and the effects of both mechanisms are observed. The total acoustic disturbance is simply the sum of Eqs. 15 and 17 with appropriately weighted amplitudes A and B. Diffracted signal at any time goes as the square of the density excursion inside the material, calculated from Eq. 16. Equations 15 through 17 predict the positions and relative amplitudes of the signal maxima for any concentration of absorbing species, and a gradual transition from data of the form in Figure 6a to that in Figure 6c is predicted and was observed for a large number of intermediate concentration solutions. The amplitude of the acoustic response to optically absorbed excitation pulses (A in Eq. 15) has been quantitatively related to the absorption strength and to thermal expansion and elastic stiffness coefficients of the sample (7, 8). The amplitude of the electrostrictively generated waves (B in Eq. 17) has been similarly related to the sample's electrostrictive (photoelastic) constants (7, 9). Comparison of the acoustic response due to a known amount of absorption to the electrostrictively generated response, using data such as that in Figure 6b, permits the accurate measurement of photoelastic constants (7).

It is of interest to note that only weak absorption is needed to produce a detectable "heating" acoustic response. For example, with YAG fundamental (1.06 μm) excitation pulses, absorption into vibrational overtones of water produces a response that obscures the electrostrictively generated response. With deuterated water (or with H_2O and 532 nm excitation), electrostriction effects dominate. Similar results have been obtained with benzene and deuterated benzene. By tuning the excitation wavelength, an overtone absorption spectrum can be taken (7). This is illustrated in Figure 7. In this experiment (7), the dye laser was used for excitation, and a green ($2\times$Nd:YAG) probe pulse was employed. The dye laser was tuned to various points across the $0\rightarrow 6$ transition of a benzene C-H stretching vibrational mode centered at 607 nm. At each wavelength the diffracted intensity of the first and second maxima in the LIPS signal from pure benzene was recorded. The data sets have the appearance of Figure 6b. From this data the absorption strength is determined. The sample path length was only 1 mm, and although the spectrum is quite noisy, it is clear that the technique has the potential for great sensitivity.

Finally, I wish to illustrate the results of LIPS ultrasonic wave generation in anisotropic media. Figure 8 shows LIPS data from the monoclinic molecular crystal α-perylene. This has been discussed in detail previously

(8, 38). Excitation and probe wavelengths were 532 nm and were weakly absorbed by the sample, leading to one oscillation per acoustic cycle. In Figures 7a and 7b, the grating was aligned along the $\bar{b}$ and $\bar{a}$ crystallographic axes, respectively, and single longitudinal waves were generated. With the grating aligned between the $\bar{a}$ and $\bar{b}$ axes in the $\bar{a}\bar{b}$ plane, quasilongitudinal and quasitransverse waves of different frequencies were generated. The theory of LIPS acoustic wave generation in anisotropic media has been detailed in Ref. (8), and predicts the observed results. In anisotropic media, pure longitudinal waves or quasilongitudinal and quasitransverse waves will be generated depending upon grating orientation. Anisotropic acoustic parameters (velocities and attenuations) can thus be measured with this technique.

The LIPS technique is an extremely versatile tool for controlled optical generation of ultrasonic waves in condensed media. LIPS experiments have been performed on transparent and absorbing solutions, organic and inorganic crystals, glasses, and plastics. The effects have been observed from liquid helium temperatures to room temperature. Acoustic waves have been generated by stimulated Brillouin scattering and by optical absorption. With a mode-locked Nd:YAG system, the acoustic frequency can be varied between about 3 MHz and 30 GHz, and above 60 GHz in some materials. Any propagation direction can be selected,

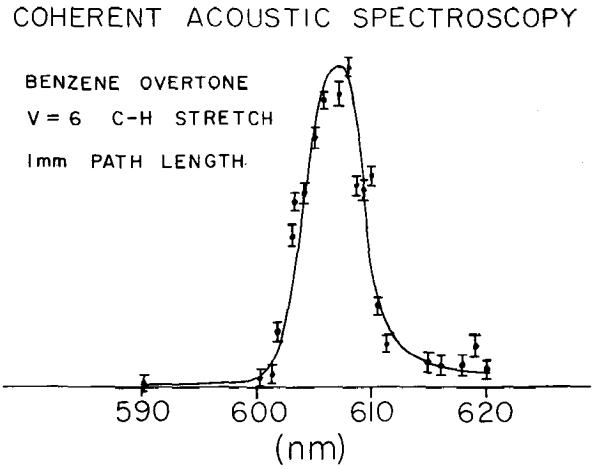

Figure 7 A spectrum of the $v = 6$ transition of a C-H stretch of benzene in a 1 mm path of pure benzene. The spectrum is obtained from the LIPS transient grating experiment as a function of excitation wavelength for fixed probe pulse wavelength. The data has an appearance like that of Figure 6b. At each wavelength the relative height of the first and second peak is determined. This relative height is proportional to the extent of absorption. Thus, the technique is a type of coherent acoustic spectroscopy.

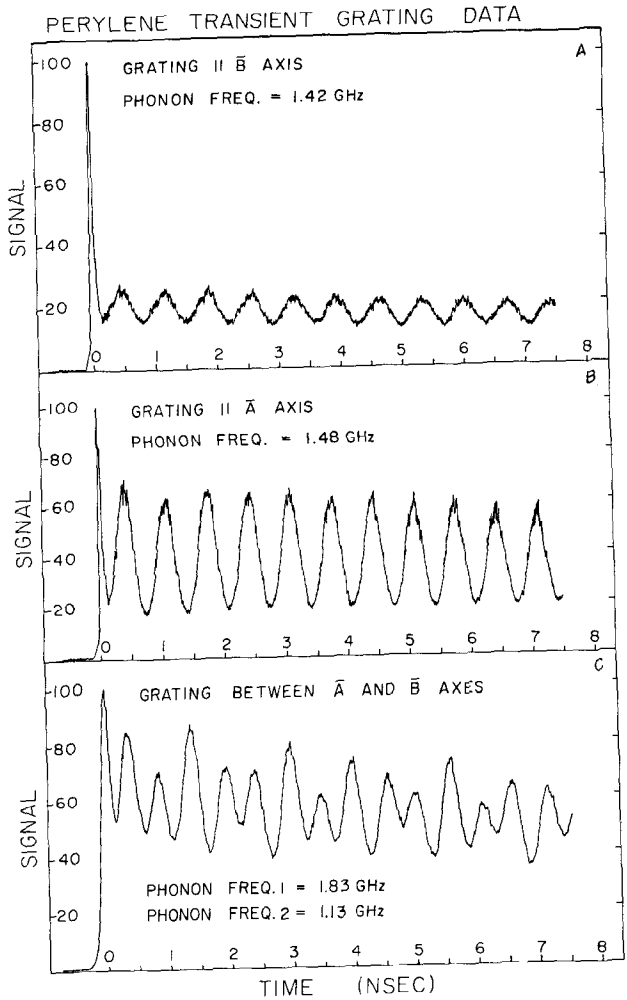

Figure 8 LIPS results for pure α-perylene. Acoustic wavelength is 1.73 μm in all cases. (*a*) Acoustic waves propagate along the $\bar{B}$ (symmetry) axis. Single-frequency modulation is observed. (*b*) Acoustic waves propagate along the $\bar{A}$ axis; single-frequency modulation is observed. (*c*) Waves propagate between $\bar{A}$ and $\bar{B}$ axes, in $\bar{A}\bar{B}$ plane. Beating is due to generation of quasilongitudinal and quasitransverse waves of identical wavelength but having different frequencies.

and in anisotropic materials quasilongitudinal and quasitransverse waves can be generated. The optically generated acoustic waves can be optically amplified, cancelled, or phase shifted (10).

There are a wide variety of applications for the LIPS effect (8–11). It has been used to measure anisotropic elastic constants. Acoustic attenuation measurements have been made. After the traveling waves leave the excitation region, only the "static" acoustic response arising from the absorbing mechanism remains. This decays slowly because of thermal diffusion, and measurement of its decay in crystals as a function of orientation can yield thermal diffusion tensors. LIPS could find possible applications in the field of optical communications. The diffracted probe beam could be both amplitude and frequency (phase) modulated to carry information. The applicability of LIPS to measure photoelastic constants and absorption spectra of weakly absorbing materials has been demonstrated. Finally, LIPS may be of great use in the nondestructive acoustic testing of a wide variety of materials for which conventional techniques are not possible. We are currently involved in making structural measurements on phospholipid bilayers and on single crystal optical fibers using these optically generated and detected acoustic effects.

CONCLUDING REMARKS

In our studies of condensed phase molecular dynamics we have found picosecond transient grating experiments to be versatile tools with a wide range of applications. Here three examples have been discussed in some detail: observation of the dispersive as well as the absorptive characters of excited states, examination of electronic excited state transport and trapping in concentrated dye solutions, and optically generated and detected acoustic wave experiments. A wide variety of other experiments were mentioned. Picosecond transient grating experiments provide new observables that will continue to contribute to an enhanced understanding of condensed phase systems.

ACKNOWLEDGMENT

The material presented in this article is based on extensive work performed in collaboration with a number of investigators. I would like to take this opportunity to thank Professor Keith A. Nelson, Dr. R. Casalegno, R. J. Dwayne Miller, Dr. C. R. Gochanour, and Dr. D. R. Lutz. Also I would like to thank the National Science Foundation, Division of Material Research for supporting the bulk of the research described in this article and the Department of Energy for support of the work on excited state dynamics in concentrated dye solutions.

Literature Cited

1. Hetherington, W. M., Michaels, R. H., Eisenthal, K. B. 1979. *Chem. Phys. Lett.* 66:230–33
2. Tredwell, C. J., Porter, G. 1978. *Chem. Phys. Lett.* 56:278–82
3. Gochanour, C. R., Fayer, M. D. 1981. *J. Phys. Chem.* 85:1989–94
4. Busch, G. E., Jones, R. P., Rentzepis, P. M. 1973. *Chem. Phys. Lett.* 18:178–85
5. Chuang, T. J., Eisenthal, K. B. 1971. *Chem. Phys. Lett.* 11:368–70
6. Lutz, D. R., Nelson, K. A., Gochanour, C. R., Fayer, M. D. 1981. *Chem. Phys.* 58:325–34
7. Miller, R. J. D., Casalegno, R., Nelson, K. A., Fayer, M. D. 1982. *Chem. Phys.* In press
8. Nelson, K. A., Fayer, M. D. 1980. *J. Chem. Phys.* 72:5202–18
9. Nelson, K. A., Lutz, D. R., Fayer, M. D. 1981. *Phys. Rev. B* 24:3261–75
10. Nelson, K. A., Miller, R. J. D., Lutz, D. R., Fayer, M. D. 1982. *J. Appl. Phys.* 53:1144–49
11. Nelson, K. A., Casalegno, R., Miller, R. J. D., Fayer, M. D. 1982. *J. Chem. Phys.* In press
12. Kogelnik, H. 1969. *Bell Syst. Tech. J.* 48:2909–13
13. Born, M., Wolf, E. 1965. *Principles of Optics*. Oxford: Pergamon. 3rd ed.
14. Scrivner, G. P., Tubbs, M. R. 1974. *Opt. Commun.* 10:32
15. Gochanour, C. R., Andersen, H. C., Fayer, M. D. 1979. *J. Chem. Phys.* 4254–71
16. Loring, R. F., Andersen, H. C., Fayer, M. D. 1982. *J. Chem. Phys.* 76:2015–27
17. Imbusch, G. F. 1967. *Phys. Rev.* 153:326–35
18. Birks, J. B. 1970. *Photophysics of Aromatic Molecules*, pp. 142–92. New York: Wiley-Interscience
19. Schäfer, F. P. 1977. In *Topics in Applied Physics*, ed. F. P. Schäfer, 1:21–24, 158–60. New York:Springer-Verlag. 2nd ed.
20. Berlman, I. 1973. *Energy Transfer Parameters of Aromatic Compounds*, p. 62. New York:Academic
21. McElroy, J. D., Feher, G., Mauzerall, D. C. 1972. *Biochim. Biophys. Acta* 267:363–67
22. Norris, J. R., Druyan, M. E., Katz, J. J. 1973. *J. Am. Chem. Soc.* 95:1680–85
23. Berlman, I. 1973. See Ref. 20, pp. 27–47, and references therein
24. Selwyn, J. E., Steinfeld, J. I. 1972. *J. Phys. Chem.* 76:762–71
25. Bojarski, C., Kuśba, J., Obermueller, G. 1975. *Acta Phys. Polon. A* 48:85–92
26. Wieting, R. D., Fayer, M. D., Dlott, D. D. 1978. *J. Chem. Phys.* 69:1996–2010
27. Montroll, E. W. 1964. *Proc. Symp. Appl. Math.* 16:193. Providence, R.I:Am. Math. Soc.
28. Montroll, E. W. 1969. *J. Math. Phys.* 10:753–59
29. Fayer, M. D. 1982. In *Modern Problems in Solid State Physics: Molecular Solids*, ed. A. A. Maradudin. Amsterdam: North Holland. In press
30. Quate, C. F., Wilkinson, D. W., Winslow, D. K. 1965. *Proc. IEEE* 53:1604–13
31. Kroll, N. M. 1965. *J. Appl. Phys.* 36:34–46
32. Cachier, G. 1971. *J. Acoust. Soc. Am.* 49:974–85
33. Yang, K. H., Richards, P. L., Shen, Y. R. 1973. *J. Appl. Phys.* 44:1417–23
34. Grill, W., Weis, O. 1975. *Phys. Rev. Lett.* 35:588–91
35. Meltzer, R. S., Rives, J. E. 1977. *Phys. Rev. Lett.* 38:421–25
36. Eichler, H., Stahl, H. 1973. *J. Appl. Phys.* 44:3429–42, and references therein
37. Altenburg, K. 1972. *Z. Phys. Chem. Leipzig* 250:399–411
38. Nelson, K. A., Dlott, D. D., Fayer, M. D. 1979. *Chem. Phys. Lett.* 64:88–93

Annual Review of Physical Chemistry
Volume 33, 1982

CONTENTS